Published for SISSA by Springer

Received: *May 10, 2019*
Revised: *August 30, 2019*
Accepted: *September 10, 2019*
Published: *October 9, 2019*

JHEP10(2019)124

A search for $\Xi_{cc}^{++} \to D^+pK^-\pi^+$ decays

The LHCb collaboration

E-mail: murdotraill@hotmail.com

Abstract: A search for the Ξ_{cc}^{++} baryon through the $\Xi_{cc}^{++} \to D^+pK^-\pi^+$ decay is performed with a data sample corresponding to an integrated luminosity of $1.7\,\text{fb}^{-1}$ recorded by the LHCb experiment in pp collisions at a centre-of-mass energy of 13 TeV. No significant signal is observed in the mass range from the kinematic threshold of the decay to $3800\,\text{MeV}/c^2$. An upper limit is set on the ratio of branching fractions $\mathcal{R} = \frac{\mathcal{B}(\Xi_{cc}^{++} \to D^+pK^-\pi^+)}{\mathcal{B}(\Xi_{cc}^{++} \to \Lambda_c^+K^-\pi^+\pi^+)}$ with $\mathcal{R} < 1.7\ (2.1) \times 10^{-2}$ at the 90% (95%) confidence level at the known mass of the Ξ_{cc}^{++} state.

Keywords: Branching fraction, Charm physics, Hadron-Hadron scattering (experiments)

ArXiv ePrint: 1905.02421

https://doi.org/10.1007/JHEP10(2019)124

Contents

JHEP10(2019)124

1 Introduction

The first observed doubly charged and doubly charmed baryon was the Ξ_{cc}^{++} (ccu) state found through the $\Xi_{cc}^{++} \to \Lambda_c^+ K^- \pi^+ \pi^+$ and $\Xi_{cc}^{++} \to \Xi_c^+ \pi^+$ decay modes by the LHCb collaboration [1, 2]. With two heavy constituent quarks, this baryon provides a unique system for testing quantum chromodynamics. The average mass of the Ξ_{cc}^{++} baryon from the two LHCb measurements now stands at 3621.24 ± 0.65 (stat) ± 0.31 (syst) MeV/c^2 and its lifetime is $0.256^{+0.024}_{-0.022}$ (stat) ± 0.014 (syst) ps [3], consistent with a weakly decaying state. However, many features of the Ξ_{cc}^{++} baryon remain unknown, including its spin and parity. Previously, signals of the singly charged Ξ_{cc}^{+} state were reported in the $\Lambda_c^+ K^- \pi^+$ and $pD^+ K^-$ final states by the SELEX collaboration [4, 5]. The masses of the Ξ_{cc}^{++} and Ξ_{cc}^{+} ground states are expected to be approximately equal according to isospin symmetry [6]. Searches in different production environments at the FOCUS, BaBar, Belle and LHCb experiments have however not shown evidence for a Ξ_{cc}^{+} state with the properties reported by the SELEX collaboration [7–10].

To further understand the dynamics of weakly decaying doubly heavy baryons, it is of prime importance to pursue searches for additional decay modes of the Ξ_{cc}^{++} baryon. These decays may differ significantly from those of singly heavy hadrons due to interference effects between decay amplitudes of the two heavy quarks. From an experimental viewpoint, the decay $\Xi_{cc}^{++} \to D^+(\to K^- \pi^+ \pi^+) p K^- \pi^+$ is a suitable search channel, since the

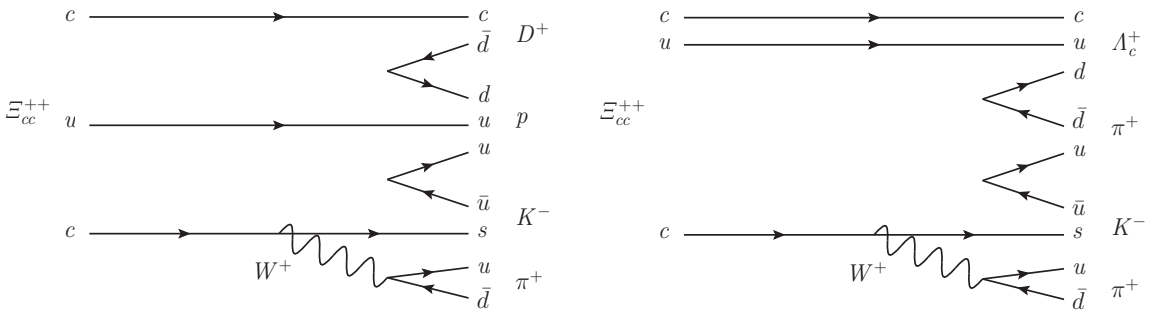

Figure 1. The Feynman diagram contributing to the inclusive (left) $\Xi_{cc}^{++} \to D^+pK^-\pi^+$ decay with the analogous (right) $\Xi_{cc}^{++} \to \Lambda_c^+K^-\pi^+\pi^+$ diagram.

$D^+ \to K^-\pi^+\pi^+$ trigger is proven to be very efficient at LHCb [11].[1] The tree-level amplitudes of the inclusive decays of $\Xi_{cc}^{++} \to D^+pK^-\pi^+$ and $\Xi_{cc}^{++} \to \Lambda_c^+K^-\pi^+\pi^+$, as shown in figure 1, are comparable, which suggests that the branching fractions of these two modes could be similar. Theoretical calculations have been performed on pseudo-two-body decays of doubly-charmed baryons [12]. The $\Xi_{cc}^{++} \to D^+pK^-\pi^+$ decay could proceed as a pseudo-two-body decay if it decays via an excited Σ^{+*} state with a mass greater than $1572\,\text{MeV}/c^2$, which would then decay to a $pK^-\pi^+$ final state. However, the properties of such Σ^{+*} decays are not well known [13]. The $\Xi_{cc}^{++} \to D^+pK^-\pi^+$ decay also has a energy release of 180 MeV, compared to 560 MeV for the $\Xi_{cc}^{++} \to \Lambda_c^+K^-\pi^+\pi^+$ decay, which means it is expected to have a lower branching fraction because of the smaller available phase space.

The analysis presented in this paper searches for the Ξ_{cc}^{++} baryon, at its known mass, through $\Xi_{cc}^{++} \to D^+pK^-\pi^+$ decays and also explores a larger mass range to identify the hypothetical isospin partner of the Ξ_{cc}^+ state that the SELEX collaboration reported. The analysis uses pp collision data corresponding to an integrated luminosity of $1.7\,\text{fb}^{-1}$ recorded by the LHCb experiment in 2016 at a centre-of-mass energy of 13 TeV. The branching fraction of the $\Xi_{cc}^{++} \to D^+pK^-\pi^+$ decay is normalised to $\Xi_{cc}^{++} \to \Lambda_c^+K^-\pi^+\pi^+$ to reduce systematic uncertainties.

The ratio of branching fractions, $\mathcal{R}$, is determined as

$$\begin{aligned}\mathcal{R} &= \frac{\mathcal{B}(\Xi_{cc}^{++} \to D^+pK^-\pi^+)}{\mathcal{B}(\Xi_{cc}^{++} \to \Lambda_c^+K^-\pi^+\pi^+)} \\ &= \frac{\mathcal{B}(\Xi_{cc}^{++} \to D^+(\to K^-\pi^+\pi^+)pK^-\pi^+)}{\mathcal{B}(\Xi_{cc}^{++} \to \Lambda_c^+(\to pK^-\pi^+)K^-\pi^+\pi^+)} \times \frac{\mathcal{B}(\Lambda_c^+ \to pK^-\pi^+)}{\mathcal{B}(D^+ \to K^-\pi^+\pi^+)} \\ &= \frac{N(D^+pK^-\pi^+)}{N(\Lambda_c^+K^-\pi^+\pi^+)} \times \frac{\varepsilon(\Lambda_c^+K^-\pi^+\pi^+)}{\varepsilon(D^+pK^-\pi^+)} \times \frac{\mathcal{B}(\Lambda_c^+ \to pK^-\pi^+)}{\mathcal{B}(D^+ \to K^-\pi^+\pi^+)},\end{aligned} \tag{1.1}$$

where $N(D^+pK^-\pi^+)$ and $N(\Lambda_c^+K^-\pi^+\pi^+)$ refer to the measured yields of the signal in the $\Xi_{cc}^{++} \to D^+pK^-\pi^+$ and $\Xi_{cc}^{++} \to \Lambda_c^+K^-\pi^+\pi^+$ channels, respectively, and $\varepsilon(D^+pK^-\pi^+)$ and $\varepsilon(\Lambda_c^+K^-\pi^+\pi^+)$ are the corresponding selection efficiencies of the decay modes. The

[1]The inclusion of charge-conjugate processes is implied throughout this paper.

JHEP10(2019)124

values for $\mathcal{B}(D^+ \to K^-\pi^+\pi^+)$ and $\mathcal{B}(\Lambda_c^+ \to pK^-\pi^+)$ are known to be $(8.98 \pm 0.28)\%$ and $(6.23 \pm 0.33)\%$, respectively [13] and are uncorrelated.

For convenience, the single-event sensitivity, α_s, is defined as

$$\alpha_s \equiv \frac{\varepsilon(\Lambda_c^+ K^-\pi^+\pi^+)}{N(\Lambda_c^+ K^-\pi^+\pi^+)\,\varepsilon(D^+pK^-\pi^+)} \times \frac{\mathcal{B}(\Lambda_c^+ \to pK^-\pi^+)}{\mathcal{B}(D^+ \to K^-\pi^+\pi^+)} \tag{1.2}$$

such that eq. (1.1) reduces to $\mathcal{R} = \alpha_s \times N(D^+pK^-\pi^+)$. All aspects of the analysis are fixed before the data in the $[3300, 3800]\,\mathrm{MeV}/c^2$ mass region are examined.

2 Detector and software

The LHCb detector [14, 15] is a single-arm forward spectrometer covering the pseudorapidity range $2 < \eta < 5$, designed for the study of particles containing b or c quarks. The detector includes a high-precision tracking system consisting of a silicon-strip vertex detector surrounding the pp interaction region [16], a large-area silicon-strip detector located upstream of a dipole magnet with a bending power of about 4 Tm, and three stations of silicon-strip detectors and straw drift tubes [17] placed downstream of the magnet. The tracking system provides a measurement of the momentum, p, of charged particles with a relative uncertainty that varies from 0.5% at low momentum to 1.0% at $200\,\mathrm{GeV}/c$. The minimum distance of a track to a primary vertex (PV), the impact parameter (IP), is measured with a resolution of $(15 + 29/p_\mathrm{T})\,\mu\mathrm{m}$, where p_T is the component of the momentum transverse to the beam, in GeV/c. Charged hadrons are identified using two ring-imaging Cherenkov detectors [18]. Photon, electron and hadron candidates are identified by a calorimeter system consisting of scintillating-pad, pre-shower detectors, an electromagnetic calorimeter and a hadronic calorimeter. Muons are identified by a system composed of alternating layers of iron and multiwire proportional chambers [19]. The trigger consists of a hardware stage, based on information from the calorimeter and muon systems, followed by a software stage, which applies a full event reconstruction. The online reconstruction incorporates near-real-time alignment and calibration of the detector [11]. The same alignment and calibration information is propagated to the offline reconstruction, ensuring consistent and high-quality information between the trigger and offline software. The identical performance of the online and offline reconstruction offers the opportunity to perform physics analyses directly using candidates reconstructed in the trigger [20]. The analysis described in this paper makes use of these features.

Simulated $\Xi_{cc}^{++} \to D^+pK^-\pi^+$ decays are used to design the candidate selection and to calculate the efficiency of such a selection. The proton-proton interactions are generated using Pythia [21] with a specific LHCb configuration [23]. Genxicc v2.0 [24], the dedicated generator for doubly-heavy-baryon production at LHCb, is used to produce the signal. Decays of hadronic particles are described by EvtGen [25], in which final-state radiation is generated using Photos [26]. The interaction of the generated particles with the detector and their response are implemented using the Geant4 toolkit [27] as described in ref. [29]. The $\Xi_{cc}^{++} \to D^+pK^-\pi^+$ decays are generated with a Ξ_{cc}^{++} mass of $3621.40\,\mathrm{MeV}/c^2$ and the decay products of Ξ_{cc}^{++} and D^+ hadrons are distributed uniformly in phase space.

JHEP10(2019)124

3 Triggering, reconstruction and selection

The procedure to trigger, reconstruct and select candidates is designed to retain Ξ_{cc}^{++} signal and to suppress three primary sources of background: combinatorial background, which arises from random combination of tracks; misreconstructed charm or beauty hadron decays, which typically have displaced decay vertices; and combinations of a real D^+ meson with other tracks to form a fake Ξ_{cc}^{++} candidate. To better control systematic uncertainties, the selection of $\Xi_{cc}^{++} \to D^+ p K^- \pi^+$ decays is also designed to be as similar as possible to that of the $\Xi_{cc}^{++} \to \Lambda_c^+ K^- \pi^+ \pi^+$ normalisation channel, described in ref. [1].

The D^+ candidates are reconstructed in the final state $K^-\pi^+\pi^+$. At least one of the three tracks used to reconstruct the D^+ candidate must be selected by the inclusive software trigger, which requires that the track has $p_{\mathrm{T}} > 250\,\mathrm{MeV}/c$ and $\chi^2_{\mathrm{IP}} > 4$ with respect to any PV, where χ^2_{IP} is defined as the difference in χ^2 of a given PV reconstructed with and without the considered track. The D^+ candidate then must be reconstructed and accepted by a dedicated $D^+ \to K^-\pi^+\pi^+$ selection algorithm in the software trigger. This algorithm applies several geometric and kinematic requirements; at least one of the three tracks must have $p_{\mathrm{T}} > 1\,\mathrm{GeV}/c$ and $\chi^2_{\mathrm{IP}} > 50$, at least two of the tracks must have $p_{\mathrm{T}} > 0.4\,\mathrm{GeV}/c$ and $\chi^2_{\mathrm{IP}} > 10$ and the scalar sum of the p_{T} of the three tracks must be larger than $3\,\mathrm{GeV}/c$. Furthermore, the D^+ candidate must have a good vertex-fit quality with $\chi^2/\mathrm{ndf} < 6$. The candidate must also point back to its associated PV, where the angle between its flight path and momentum vector should be less than 0.01 radians. The associated PV is that which best fits the flight direction of the reconstructed candidate. The D^+ vertex must also be displaced from this PV such that the estimated D^+ decay time is longer than 0.4 ps. Only candidates whose invariant mass is within $\pm 80\,\mathrm{MeV}/c^2$ of the known mass of the D^+ meson ($1869.65\,\mathrm{MeV}/c^2$ [13]) are retained. Finally, candidates are required to pass a MatrixNet classifier [11] within the software trigger, which has been trained on p_{T} and vertex χ^2 information prior to data taking. For events that pass the online trigger, the offline selection of D^+ candidates proceeds in a similar fashion to that used in the software trigger: three tracks are required to form a common vertex that is significantly displaced from the associated PV of the candidate and its combined invariant mass must be in the range $[1847, 1891]\,\mathrm{MeV}/c^2$. Particle identification (PID) requirements are imposed on all three tracks to suppress combinatorial background and misidentified charm decays. The Ξ_{cc}^{++} candidates are formed by combining a D^+ candidate with three more charged tracks, each with $p_{\mathrm{T}} > 500\,\mathrm{MeV}/c$ and separately identified as a proton, kaon and pion with good track quality. The three tracks and the D^+ candidate are required to form a vertex in which each pairwise combination of the four particles is required to have a distance of closest approach of less than 10 mm and the fitted Ξ_{cc}^{++} vertex must have $\chi^2/\mathrm{ndf} < 10$. The Ξ_{cc}^{++} candidate is also required to point back to the PV, and to have $p_{\mathrm{T}} > 4.5\,\mathrm{GeV}/c$. Only events that passed the hardware trigger based on information from the muon and calorimeter systems that are not part of the reconstructed Ξ_{cc}^{++} event are used in the analysis [11]. Hence, the event is triggered independently of the reconstructed Ξ_{cc}^{++} candidate, which reduces the systematic uncertainty on the efficiency ratios between the $\Xi_{cc}^{++} \to D^+ p K^- \pi^+$ and $\Xi_{cc}^{++} \to \Lambda_c^+ K^- \pi^+ \pi^+$ decay modes.

JHEP10(2019)124

To improve the mass resolution, the following mass estimator is used in the analysis

$$m(D^+pK^-\pi^+) \equiv M(D^+pK^-\pi^+) - M([K^-\pi^+\pi^+]_{D^+}) + M_{\rm PDG}(D^+), \tag{3.1}$$

where $M(D^+pK^-\pi^+)$ is the measured invariant mass of the Ξ_{cc}^{++} candidate, $M([K^-\pi^+\pi^+]_{D^+})$ is the measured invariant mass of the $K^-\pi^+\pi^+$ combination corresponding to the intermediate D^+ candidate and $M_{\rm PDG}(D^+)$ is the known mass of the D^+ meson. By using the mass definition in eq. (3.1), a mild correlation between decay time and mass is reduced and the mass resolution is improved by $0.15\,\text{MeV}/c^2$. The Ξ_{cc}^{++} candidates are accepted if they have a reconstructed mass in the range $3300 \leq m(D^+pK^-\pi^+) \leq 3800\,\text{MeV}/c^2$.

Following a comparison study of different multivariate methods, a classifier based on the multilayer perceptron (MLP) algorithm [30] is used to further suppress combinatorial background. Simulated Ξ_{cc}^{++} decays are used to train the MLP classifier to recognise signal. Dedicated software triggers reconstruct an unphysical combination of $D^+pK^+\pi^+$ (wrong-sign-plus, WSP) and $D^+pK^-\pi^-$ (wrong-sign-minus, WSM) data. The WSP and WSM samples are expected to be good proxies for combinatorial background in the $\Xi_{cc}^{++} \to D^+pK^-\pi^+$ (right-sign, RS) channel. For this analysis, WSP data in the $3550 \leq m(D^+pK^-\pi^+) \leq 3700\,\text{MeV}/c^2$ mass region is used to train the MLP classifier to identify background, while the WSM data is used to cross-check the results. Fifteen input variables are used in the MLP training. The variables with the best discriminating power between signal and background are: the Ξ_{cc}^{++} vertex fit with a kinematic refit [31] of the Ξ_{cc}^{++} decay chain requiring it to originate from its PV; the smallest $p_{\rm T}$ of the four decay products of the Ξ_{cc}^{++} candidate; the angle between the Ξ_{cc}^{++} momentum vector and the direction from the PV to the Ξ_{cc}^{++} decay vertex; the $\chi^2_{\rm IP}$ of the Ξ_{cc}^{++} candidate with respect to its PV; the maximum distance of the closest approach between all pairs of Ξ_{cc}^{++} tracks forming the Ξ_{cc}^{++} candidate; and the maximum distance of the closest approach between all pairs of tracks from the decay of the D^+ candidate. To maintain a sizeable number of signal events, the hardware-trigger requirements are not applied to the signal and background samples. In addition to the training samples, disjoint testing samples are acquired from the same source. After training, the response of the MLP is compared between the training and testing samples. No signs of the MLP classifier being overtrained are found based on the Kolmogorov-Smirnov test statistic. Candidates are retained only if the MLP response output exceeds a certain threshold. The threshold is chosen by maximising the Punzi figure of merit [32], with a target significance of five sigma. To test for potential misreconstruction effects, the same selection criteria are applied to the WSP and WSM data; no peaking structures are visible in either control sample, as expected.

After the multivariate selection, events may contain multiple Ξ_{cc}^{++} candidates. This can arise from mistakes in the reconstruction of $\Xi_{cc}^{++} \to D^+(\to K^-\pi^+\pi^+)pK^-\pi^+$ decays. For instance, there can be cases when Ξ_{cc}^{++} candidates in the same event have used the same track more than once. To deal with this, the angle between any two tracks of the same charge is required to be greater than 0.5 mrad. If a Ξ_{cc}^{++} candidate has been formed from at least one pair of these cloned tracks, then the candidate is removed. This requirement removes around 6% of Ξ_{cc}^{++} candidates in RS data following the multivariate selection. In a separate scenario, the same six final-state tracks may be used to reconstruct more

JHEP10(2019)124

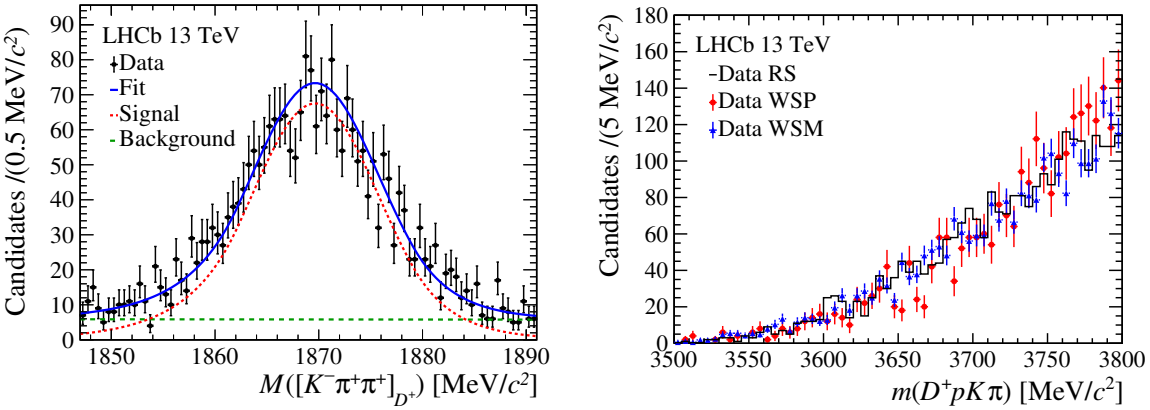

Figure 2. (Left) Invariant-mass distribution of the D^+ candidates after the full selection. The black points represent data and the fit is indicated by the continuous (blue) line with the individual signal and background components represented by the dotted (red) line and dashed (green) line, respectively. (Right) Invariant-mass distributions of right-sign (black) $D^+pK^-\pi^+$, wrong-sign-plus (red) $D^+pK^+\pi^+$ and wrong-sign-minus (blue) $D^+pK^-\pi^-$ data combinations are shown. The control samples have been normalised to the right-sign sample.

than one Ξ_{cc}^{++} candidate in the same event but with the tracks wrongly interchanged (e.g., the K^- track originating from the Ξ_{cc}^{++} decay vertex and the K^- track coming from the D^+ decay vertex). In this situation, only one of the Ξ_{cc}^{++} candidate from such an event, chosen at random, is retained. This requirement discards less than 1% of candidates at this stage of the selection.

4 Mass distributions

To determine the yield of Ξ_{cc}^{++} and D^+ particles following the selection of $\Xi_{cc}^{++}\to D^+pK^-\pi^+$ candidates, the $m(D^+pK^-\pi^+)$ and $M([K^-\pi^+\pi^+]_{D^+})$ mass distributions are fitted using models that are developed using simulation.

The invariant-mass distribution $M([K^-\pi^+\pi^+]_{D^+})$ of the D^+ candidates after the candidate selection is shown in figure 2 (left). A Crystal Ball function with exponential tails on both sides [33] is used to model the signal component and a linear function is used to fit the background contribution. The parameters of the signal model are fixed to values obtained from simulation, while all parameters in the background model are free. The selection retains 2697 D^+ candidates with a purity of 80% according to the results of the fit to the mass spectrum.

The invariant-mass distributions in the RS, WSP and WSM data samples after the candidate selection are shown in figure 2 (right). All the samples have similar smoothly shaped distributions across the entire mass range studied.

The invariant-mass distribution of the Ξ_{cc}^{++} candidates, $m(D^+pK^-\pi^+)$, for the signal decay mode after applying all requirements of the analysis, is shown in figure 3 (left). The mass distribution is fitted with an unbinned extended maximum-likelihood method, assuming only a background contribution, described by a second-order Chebyshev polynomial.

JHEP10(2019)124

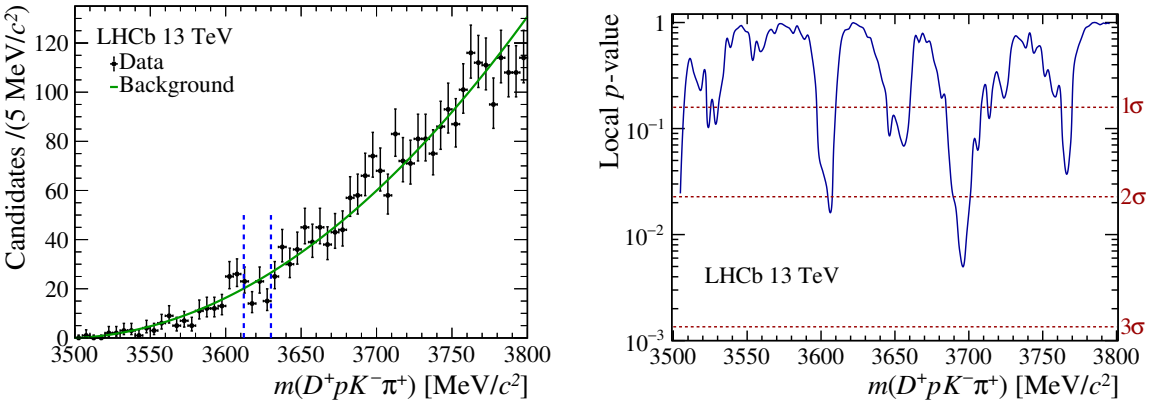

Figure 3. (Left) Invariant-mass distribution of the $\Xi_{cc}^{++} \to D^+pK^-\pi^+$ candidates with the fit overlaid. The black points represent data, the continuous (green) line represents the combinatorial background and the two vertical parallel dashed (blue) lines define the region where the signal is expected. (Right) The local p-value expressing the compatibility of the data with the background-only hypothesis. The horizontal dashed (red) lines indicate p-values of 1, 2 and 3σ local significance.

No signal peak is visible in the spectrum and the local p-value is calculated as a function of mass and shown in figure 3 (right). The local p-value is defined as the probability of observing data that is less compatible with the background-only hypothesis than the data set. The test statistic used is based on q_0 in ref. [34], but instead of assigning it the value zero when observing fewer than expected candidates, it is assigned the value $-q_0$ to achieve a more intuitive behaviour of the p-value for downward fluctuations. The likelihoods are evaluated with Poisson statistics using the predicted number of background candidates and observed number of signal candidates in regions of $\pm 3\sigma_m$ around each hypothetical mass, where $\sigma_m = 2.8\,\text{MeV}/c^2$ is the Ξ_{cc}^{++} mass resolution determined from simulated $\Xi_{cc}^{++} \to D^+pK^-\pi^+$ decays.

There is no visible signal near the mass of $3620\,\text{MeV}/c^2$ where a Ξ_{cc}^{++} signal would be expected, nor is there any excess of candidates near the mass of $3520\,\text{MeV}/c^2$ where the hypothetical isospin partner was observed by the SELEX collaboration [4, 5]. The global p-value, including the look-elsewhere effect in the mass range 3500–3800 MeV/c^2, is 26% and only one signal candidate is observed in the mass range from the kinematic threshold of $3441\,\text{MeV}/c^2$ to $3500\,\text{MeV}/c^2$. Hence, no significant signal is observed in the mass range from the kinematic threshold to $3800\,\text{MeV}/c^2$ and we proceed to set a limit on the relative branching fraction $\mathcal{R}$.

The invariant-mass distribution of the Ξ_{cc}^{++} candidates, $m(\Lambda_c^+K^-\pi^+\pi^+)$, for the normalization decay mode, $\Xi_{cc}^{++} \to \Lambda_c^+K^-\pi^+\pi^+$, is shown in figure 4. In this case a signal peak is clearly visible. Both the candidate selection and the modelling of the mass spectrum are identical to that in ref. [1], except for the additional requirements on the hardware trigger. An extended unbinned maximum-likelihood fit to this invariant-mass distribution returns a signal yield of 184 ± 29.

JHEP10(2019)124

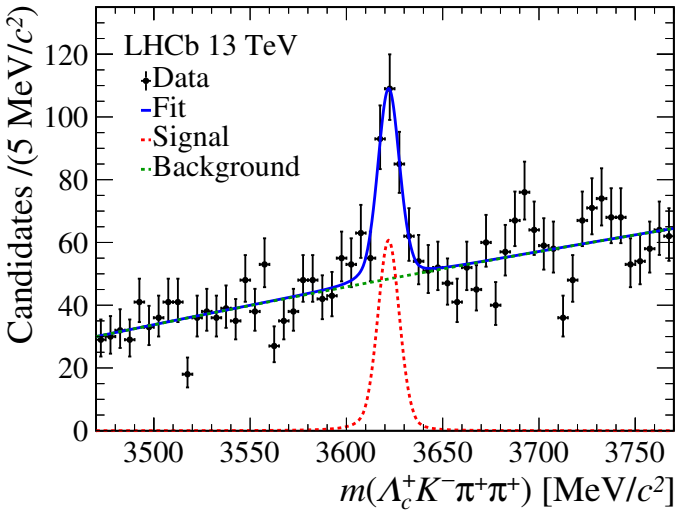

Figure 4. Invariant-mass distribution of the $\Xi_{cc}^{++} \to \Lambda_c^+ K^-\pi^+\pi^+$ candidates with the fit overlaid. The black points represent data, the dashed (green) line represents combinatorial background, the dotted (red) line represents the signal contribution and the continuous (blue) line is the total fit.

5 Efficiency determination

To set an upper limit on the ratio $\mathcal{R}$, it is necessary to evaluate the ratio of efficiencies between the $\Xi_{cc}^{++} \to D^+pK^-\pi^+$ and $\Xi_{cc}^{++} \to \Lambda_c^+K^-\pi^+\pi^+$ decay modes.

The efficiency ratio may be factorised as

$$\frac{\varepsilon(\Lambda_c^+K^-\pi^+\pi^+)}{\varepsilon(D^+pK^-\pi^+)} = \frac{\varepsilon^{\text{acc}}_{\Lambda_c^+K^-\pi^+\pi^+}}{\varepsilon^{\text{acc}}_{D^+pK^-\pi^+}} \frac{\varepsilon^{\text{sel|acc}}_{\Lambda_c^+K^-\pi^+\pi^+}}{\varepsilon^{\text{sel|acc}}_{D^+pK^-\pi^+}} \frac{\varepsilon^{\text{PID|sel}}_{\Lambda_c^+K^-\pi^+\pi^+}}{\varepsilon^{\text{PID|sel}}_{D^+pK^-\pi^+}} \frac{\varepsilon^{\text{trig|PID}}_{\Lambda_c^+K^-\pi^+\pi^+}}{\varepsilon^{\text{trig|PID}}_{D^+pK^-\pi^+}}, \tag{5.1}$$

where efficiencies are evaluated for the geometric acceptance (acc), the reconstruction and selection excluding particle identification requirements (sel), the particle identification requirements (PID) and the trigger (trig). Each factor is the efficiency relative to all previous steps in the order given above. The individual ratios are evaluated with simulated Ξ_{cc}^{++} decays, assuming a uniform phase space model, except for PID which is derived from data [18, 35]. The efficiencies are corrected for known differences between simulation and data, apart from the geometric acceptance.

The individual efficiency components, shown in eq. (5.1), are found to be similar between the two Ξ_{cc}^{++} decay modes, except for the reconstruction and selection efficiency, $\varepsilon^{\text{sel|acc}}$, where in the $\Xi_{cc}^{++} \to D^+pK^-\pi^+$ channel it is found to be approximately twice as large as that of the $\Xi_{cc}^{++} \to \Lambda_c^+K^-\pi^+\pi^+$ decay. This leads to a total efficiency ratio of $\varepsilon(\Lambda_c^+K^-\pi^+\pi^+)/\varepsilon(D^+pK^-\pi^+) = 0.46 \pm 0.01$, where the uncertainty is statistical only. Combining this total relative efficiency with the value for $N(\Lambda_c^+K^-\pi^+\pi^+)$ obtained in section 4 and the known values for the branching fractions $\mathcal{B}(D^+ \to K^-\pi^+\pi^+)$ and $\mathcal{B}(\Lambda_c^+ \to pK^-\pi^+)$, then according to eq. (1.2), the single-event sensitivity is $\alpha_s = (1.74 \pm 0.29) \times 10^{-3}$. The uncertainty on α_s includes the total uncertainty

JHEP10(2019)124

on the $\mathcal{B}(D^+ \to K^-\pi^+\pi^+)$ and $\mathcal{B}(\Lambda_c^+ \to pK^-\pi^+)$ branching fractions and the statistical uncertainty on the $N(\Lambda_c^+ K^-\pi^+\pi^+)$ and $\varepsilon(\Lambda_c^+ K^-\pi^+\pi^+)/\varepsilon(D^+ pK^-\pi^+)$ measured values.

6 Systematic uncertainties

The statistical uncertainty on the measured signal yield in the $\Xi_{cc}^{++} \to \Lambda_c^+ K^-\pi^+\pi^+$ channel is the dominant uncertainty on α_s and the systematic uncertainties on α_s have small effect on the upper limits on the ratio $\mathcal{R}$.

The largest systematic uncertainty arises from the evaluation of the efficiency of the hardware-trigger requirement. Only candidates that are triggered independently of the Ξ_{cc}^{++} candidate's final-state tracks are used in the branching fraction ratio limit to minimise this systematic uncertainty. The ratio of these efficiencies is equal to one if the kinematic distributions of the Ξ_{cc}^{++} candidate in the $\Xi_{cc}^{++} \to D^+ pK^-\pi^+$ and $\Xi_{cc}^{++} \to \Lambda_c^+ K^-\pi^+\pi^+$ decay modes are identical. However, the efficiencies can be different if the respective selection requirements of the $\Xi_{cc}^{++} \to D^+ pK^-\pi^+$ and $\Xi_{cc}^{++} \to \Lambda_c^+ K^-\pi^+\pi^+$ analyses select different kinematic regions of the Ξ_{cc}^{++} candidate. This effect is studied by weighting the p_{T} distributions in simulated samples. The change in efficiency of the hardware trigger after the weighting is evaluated and results in a systematic uncertainty of 3.5%. The impact of the model used to fit the $m(\Lambda_c^+ K^-\pi^+\pi^+)$ invariant-mass distribution on the yield of Ξ_{cc}^{++} candidates, $N(\Lambda_c^+ K^-\pi^+\pi^+)$, is investigated by using alternative signal and background models and performing the fit over different mass ranges. The largest variation in the yield of Ξ_{cc}^{++} candidates is 3.1% and this is taken as a systematic uncertainty on α_s. The effect of the uncertainty associated with the Ξ_{cc}^{++} baryon's lifetime on the relative reconstruction and selection efficiency between the $\Xi_{cc}^{++} \to D^+ pK^-\pi^+$ and $\Xi_{cc}^{++} \to \Lambda_c^+ K^-\pi^+\pi^+$ channels is investigated by varying the lifetime within its uncertainty and a systematic uncertainty of 2.9% is assigned to the α_s parameter. The PID efficiency is determined in bins of particle momentum and pseudorapidity using calibration samples taken from data [35]. The size of the bins is increased or decreased by a factor of two and the largest deviation on α_s of 1.5% is assigned as systematic uncertainty. Finally, since the simulation may not describe the signal perfectly, simulated $\Xi_{cc}^{++} \to D^+ pK^-\pi^+$ decays are weighted to make their p_{T} distribution match that observed in the $\Xi_{cc}^{++} \to \Lambda_c^+ K^-\pi^+\pi^+$ data. The selection and software-trigger efficiencies are similarly calculated using p_{T}-corrected simulated Ξ_{cc}^{++} decays. The number of p_{T} bins used is increased or decreased by a factor of two and the efficiencies are recalculated for both decay channels. This results in a change in α_s of 1.2%. All efficiencies calculated from simulation are averaged over the entire phase space assuming a uniform distribution for both the $\Xi_{cc}^{++} \to D^+ pK^-\pi^+$ and $\Xi_{cc}^{++} \to \Lambda_c^+ K^-\pi^+\pi^+$ decays. The phase-space distributions of the selected candidates are uniform and show agreement in data and simulation. Therefore, no systematic uncertainty is assigned to the relative selection and reconstruction efficiencies for the effect of intermediate resonances in their decay.

Table 1 summarises the systematic and statistical uncertainties on α_s. The statistical uncertainty is dominated by the uncertainty of the yield of the normalisation mode but includes a small contribution from the finite size of the simulated samples. The ratio of

JHEP10(2019)124

Source	α_s (%)
Statistical	15.7
Branching fractions	5.7
Trigger efficiency	3.5
Mass fit model	3.1
Ξ_{cc}^{++} lifetime	2.9
PID calibration	1.5
Simulation modelling	1.2
Total uncertainty	17.7

Table 1. Systematic and statistical uncertainties on the single-event sensitivity α_s.

the branching fractions $\mathcal{B}(D^+ \to K^-\pi^+\pi^+)$ and $\mathcal{B}(\Lambda_c^+ \to pK^-\pi^+)$ have a combined uncertainty of 5.7%. The systematic uncertainties from the different sources discussed above are considered uncorrelated and are added in quadrature to give a total systematic uncertainty of 5.8%. Adding all sources of uncertainty in quadrature gives a total uncertainty of 17.7% on the α_s parameter.

7 Results

In this analysis no significant $\Xi_{cc}^{++} \to D^+pK^-\pi^+$ signal is observed so an upper limit is set on the ratio of branching fractions, $\mathcal{R}$. The `CLs` method [36] is used to determine the ratio of confidence levels (CL) between the signal-plus-background and background-only hypotheses. The upper limit is obtained from the total number of candidates, $N_{\rm obs}$, observed in the expected signal mass region. This value is calculated by counting the number of candidates within the mass region, $3612 < m(D^+pK^-\pi^+) < 3630\,\mathrm{MeV}/c^2$ (indicated by two dashed blue lines in the left-hand plot of figure 3). This mass region corresponds to approximately $\pm 3\sigma_m$ around the average mass of the Ξ_{cc}^{++} state.

The `CLs` score for a possible value of ratio $\mathcal{R}$ is calculated as

$$\texttt{CLs} = \frac{P(N_{\rm b} + N_{\rm s} \leq N_{\rm obs})}{P(N_{\rm b} \leq N_{\rm obs})}, \tag{7.1}$$

where $N_{\rm s}$ is sampled from the distribution of the expected number of signal candidates for a given ratio $\mathcal{R}$, $N_{\rm b}$ is sampled from the distribution of the expected number of background candidates predicted by the background-only fit (figure 3, left) and P indicates the probability that these statistical quantities are smaller than $N_{\rm obs}$. The data points in the mass region $3612 < m(D^+pK^-\pi^+) < 3630\,\mathrm{MeV}/c^2$ are removed for the fit and $N_{\rm b}$ is determined by performing an integral extrapolation. The probability requirements in the numerator and denominator of eq. (7.1) are tested by running a large number of pseudoexperiments sampling from a Poisson distribution with statistical means of $N_{\rm b} + N_{\rm s}$ and $N_{\rm b}$, respectively. The 17.7% uncertainty on α_s is fully accounted for by sampling from a Gaussian distribution in each pseudoexperiment.

The derived `CLs` curve as a function of the possible values of the ratio $\mathcal{R}$ is shown as the black line in figure 5. This curve is obtained using values of $N_{\rm obs} = 66$ and $N_{\rm b} = 79.8$ as

JHEP10(2019)124

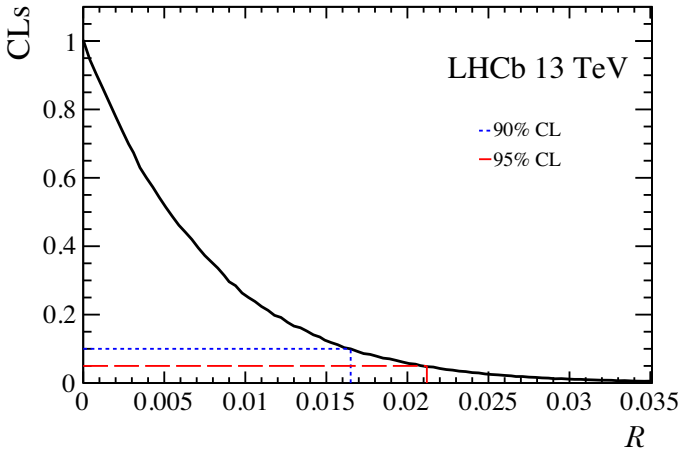

Figure 5. The scores from the `CLs` method for each value of the assumed ratio of branching fractions $\mathcal{R}$. Observed values are shown by the solid black line. The set upper limits at 90% and 95% CL are indicated by the dotted (blue) line and the dashed (red) line, respectively.

observables and running 1×10^6 pseudoexperiments for each hypothetical value of ratio $\mathcal{R}$. The upper limit measured is

$$\mathcal{R} < 1.7\ (2.1) \times 10^{-2}\ \text{at}\ 90\%\ (95\%)\ \text{CL}$$

as shown by the blue dotted line (red dashed line) in figure 5.

8 Conclusions

Following observations of the $\Xi_{cc}^{++} \to \Lambda_c^+ K^- \pi^+ \pi^+$ and $\Xi_{cc}^{++} \to \Xi_c^+ \pi^+$ decay modes, a search for the decay $\Xi_{cc}^{++} \to D^+ p K^- \pi^+$ is performed using pp collision data recorded by the LHCb experiment in 2016 at a centre-of-mass energy of 13 TeV, corresponding to an integrated luminosity of $1.7\,\text{fb}^{-1}$. No significant signal is found in the mass range from the kinematic threshold of the decay of $3441\,\text{MeV}/c^2$ to $3800\,\text{MeV}/c^2$. Considering the statistical and systematic uncertainties, an upper limit on the ratio of branching fractions between the $\Xi_{cc}^{++} \to D^+ p K^- \pi^+$ and $\Xi_{cc}^{++} \to \Lambda_c^+ K^- \pi^+ \pi^+$ decay is set to be $\mathcal{R} < 1.7\ (2.1) \times 10^{-2}$ at the 90% (95%) confidence level at the known mass of the Ξ_{cc}^{++} baryon.

The upper limit on the ratio of branching fractions between the two Ξ_{cc}^{++} decay modes is derived assuming a uniform phase space model in the efficiency determinations. A better theoretical understanding of the resonant and nonresonant contributions underpinning the $\Xi_{cc}^{++} \to D^+ p K^- \pi^+$ and $\Xi_{cc}^{++} \to \Lambda_c^+ K^- \pi^+ \pi^+$ decay processes is required to understand the at least two orders of magnitude difference between the branching fractions of the two Ξ_{cc}^{++} decay modes. Dynamical effects or spin constraints in the resonance structures could be suppressing the $\Xi_{cc}^{++} \to D^+ p K^- \pi^+$ decay. The full dataset from LHCb, or future data taking with the upgraded detector, may reveal evidence of this decay and then shed more light on the production and decay dynamics of the Ξ_{cc}^{++} baryon.

JHEP10(2019)124

Acknowledgments

We express our gratitude to our colleagues in the CERN accelerator departments for the excellent performance of the LHC. We thank the technical and administrative staff at the LHCb institutes. We acknowledge support from CERN and from the national agencies: CAPES, CNPq, FAPERJ and FINEP (Brazil); MOST and NSFC (China); CNRS/IN2P3 (France); BMBF, DFG and MPG (Germany); INFN (Italy); NWO (Netherlands); MNiSW and NCN (Poland); MEN/IFA (Romania); MSHE (Russia); MinECo (Spain); SNSF and SER (Switzerland); NASU (Ukraine); STFC (United Kingdom); DOE NP and NSF (U.S.A.). We acknowledge the computing resources that are provided by CERN, IN2P3 (France), KIT and DESY (Germany), INFN (Italy), SURF (Netherlands), PIC (Spain), GridPP (United Kingdom), RRCKI and Yandex LLC (Russia), CSCS (Switzerland), IFIN-HH (Romania), CBPF (Brazil), PL-GRID (Poland) and OSC (U.S.A.). We are indebted to the communities behind the multiple open-source software packages on which we depend. Individual groups or members have received support from AvH Foundation (Germany); EPLANET, Marie Skłodowska-Curie Actions and ERC (European Union); ANR, Labex P2IO and OCEVU, and Région Auvergne-Rhône-Alpes (France); Key Research Program of Frontier Sciences of CAS, CAS PIFI, and the Thousand Talents Program (China); RFBR, RSF and Yandex LLC (Russia); GVA, XuntaGal and GENCAT (Spain); the Royal Society and the Leverhulme Trust (United Kingdom).

References

[1] LHCb collaboration, *Observation of the doubly charmed baryon* Ξ_{cc}^{++}, *Phys. Rev. Lett.* **119** (2017) 112001 [arXiv:1707.01621] [INSPIRE].

[2] LHCb collaboration, *First Observation of the Doubly Charmed Baryon Decay* $\Xi_{cc}^{++} \to \Xi_c^+\pi^+$, *Phys. Rev. Lett.* **121** (2018) 162002 [arXiv:1807.01919] [INSPIRE].

[3] LHCb collaboration, *Measurement of the Lifetime of the Doubly Charmed Baryon* Ξ_{cc}^{++}, *Phys. Rev. Lett.* **121** (2018) 052002 [arXiv:1806.02744] [INSPIRE].

[4] SELEX collaboration, *First Observation of the Doubly Charmed Baryon* Ξ_{cc}^{+}, *Phys. Rev. Lett.* **89** (2002) 112001 [hep-ex/0208014] [INSPIRE].

[5] SELEX collaboration, *Confirmation of the double charm baryon* $\Xi_{cc}^{+}(3520)$ *via its decay to* pD^+K^-, *Phys. Lett.* **B 628** (2005) 18 [hep-ex/0406033] [INSPIRE].

[6] M. Karliner and J.L. Rosner, *Isospin splittings in baryons with two heavy quarks*, *Phys. Rev.* **D 96** (2017) 033004 [arXiv:1706.06961] [INSPIRE].

[7] S.P. Ratti, *New results on c-baryons and a search for cc-baryons in FOCUS*, *Nucl. Phys. Proc. Suppl.* **115** (2003) 33 [INSPIRE].

[8] BaBar collaboration, *Search for doubly charmed baryons* Ξ_{cc}^{+} *and* Ξ_{cc}^{++} *in BABAR*, *Phys. Rev.* **D 74** (2006) 011103 [hep-ex/0605075] [INSPIRE].

JHEP10(2019)124

[9] Belle collaboration, *Observation of new states decaying into $\Lambda_c^+ K^- \pi^+$ and $\Lambda_c^+ K_S^0 \pi^-$*, *Phys. Rev. Lett.* **97** (2006) 162001 [hep-ex/0606051] [INSPIRE].

[10] LHCb collaboration, *Search for the doubly charmed baryon Ξ_{cc}^+*, *JHEP* **12** (2013) 090 [arXiv:1310.2538] [INSPIRE].

[11] LHCb collaboration, *Design and performance of the LHCb trigger and full real-time reconstruction in Run 2 of the LHC*, 2019 *JINST* **14** P04013 [arXiv:1812.10790] [INSPIRE].

[12] F.-S. Yu, H.-Y. Jiang, R.-H. Li, C.-D. Lü, W. Wang and Z.-X. Zhao, *Discovery Potentials of Doubly Charmed Baryons*, *Chin. Phys.* **C 42** (2018) 051001 [arXiv:1703.09086] [INSPIRE].

[13] Particle Data Group collaboration, *Review of Particle Physics*, *Phys. Rev.* **D 98** (2018) 030001 [INSPIRE].

[14] LHCb collaboration, *The LHCb Detector at the LHC*, 2008 *JINST* **3** S08005 [INSPIRE].

[15] LHCb collaboration, *LHCb Detector Performance*, *Int. J. Mod. Phys.* **A 30** (2015) 1530022 [arXiv:1412.6352] [INSPIRE].

[16] R. Aaij et al., *Performance of the LHCb Vertex Locator*, 2014 *JINST* **9** P09007 [arXiv:1405.7808] [INSPIRE].

[17] P. d'Argent et al., *Improved performance of the LHCb Outer Tracker in LHC Run 2*, 2017 *JINST* **12** P11016 [arXiv:1708.00819] [INSPIRE].

[18] M. Adinolfi et al., *Performance of the LHCb RICH detector at the LHC*, *Eur. Phys. J.* **C 73** (2013) 2431 [arXiv:1211.6759] [INSPIRE].

[19] A.A. Alves Jr. et al., *Performance of the LHCb muon system*, 2013 *JINST* **8** P02022 [arXiv:1211.1346] [INSPIRE].

[20] R. Aaij et al., *Tesla: an application for real-time data analysis in High Energy Physics*, *Comput. Phys. Commun.* **208** (2016) 35 [arXiv:1604.05596] [INSPIRE].

[21] T. Sjöstrand, S. Mrenna and P.Z. Skands, *A Brief Introduction to PYTHIA 8.1*, *Comput. Phys. Commun.* **178** (2008) 852 [arXiv:0710.3820] [INSPIRE].

[22] T. Sjöstrand, S. Mrenna and P.Z. Skands, *PYTHIA 6.4 Physics and Manual*, *JHEP* **05** (2006) 026 [hep-ph/0603175] [INSPIRE].

[23] LHCb collaboration, *Handling of the generation of primary events in Gauss, the LHCb simulation framework*, *J. Phys. Conf. Ser.* **331** (2011) 032047 [INSPIRE].

[24] C.-H. Chang, J.-X. Wang and X.-G. Wu, *GENXICC2.0: An Upgraded Version of the Generator for Hadronic Production of Double Heavy Baryons Ξ_{cc}, Ξ_{bc} and Ξ_{bb}*, *Comput. Phys. Commun.* **181** (2010) 1144 [arXiv:0910.4462] [INSPIRE].

[25] D.J. Lange, *The EvtGen particle decay simulation package*, *Nucl. Instrum. Meth.* **A 462** (2001) 152 [INSPIRE].

[26] P. Golonka and Z. Was, *PHOTOS Monte Carlo: A Precision tool for QED corrections in Z and W decays*, *Eur. Phys. J.* **C 45** (2006) 97 [hep-ph/0506026] [INSPIRE].

[27] GEANT4 collaboration, *Geant4 developments and applications*, *IEEE Trans. Nucl. Sci.* **53** (2006) 270 [INSPIRE].

[28] GEANT4 collaboration, *GEANT4: A Simulation toolkit*, *Nucl. Instrum. Meth.* **A 506** (2003) 250 [INSPIRE].

JHEP10(2019)124

[29] LHCb collaboration, *The LHCb simulation application, Gauss: Design, evolution and experience*, *J. Phys. Conf. Ser.* **331** (2011) 032023 [INSPIRE].

[30] H. Voss, A. Hoecker, J. Stelzer and F. Tegenfeldt, *TMVA — Toolkit for Multivariate Data Analysis with ROOT*, PoS(ACAT)040 (2007).

[31] W.D. Hulsbergen, *Decay chain fitting with a Kalman filter*, *Nucl. Instrum. Meth.* **A 552** (2005) 566 [physics/0503191] [INSPIRE].

[32] G. Punzi, *Sensitivity of searches for new signals and its optimization*, *eConf* **C 030908** (2003) MODT002 [physics/0308063] [INSPIRE].

[33] T. Skwarnicki, *A study of the radiative cascade transitions between the Upsilon-prime and Upsilon resonances*, Ph.D. Thesis, Institute of Nuclear Physics, Krakow Poland (1986) [DESY-F31-86-02] [INSPIRE].

[34] G. Cowan, K. Cranmer, E. Gross and O. Vitells, *Asymptotic formulae for likelihood-based tests of new physics*, *Eur. Phys. J.* **C 71** (2011) 1554 [*Erratum ibid.* **C 73** (2013) 2501] [arXiv:1007.1727] [INSPIRE].

[35] L. Anderlini et al., *The PIDCalib package*, LHCb-PUB-2016-021 (2016).

[36] A.L. Read, *Presentation of search results: The CL_s technique*, *J. Phys.* **G 28** (2002) 2693 [INSPIRE].

JHEP10(2019)124

The LHCb collaboration

R. Aaij[29], C. Abellán Beteta[46], B. Adeva[43], M. Adinolfi[50], C.A. Aidala[77], Z. Ajaltouni[7], S. Akar[61], P. Albicocco[20], J. Albrecht[12], F. Alessio[44], M. Alexander[55], A. Alfonso Albero[42], G. Alkhazov[35], P. Alvarez Cartelle[57], A.A. Alves Jr[43], S. Amato[2], Y. Amhis[9], L. An[19], L. Anderlini[19], G. Andreassi[45], M. Andreotti[18], J.E. Andrews[62], F. Archilli[29], J. Arnau Romeu[8], A. Artamonov[41], M. Artuso[63], K. Arzymatov[39], E. Aslanides[8], M. Atzeni[46], B. Audurier[24], S. Bachmann[14], J.J. Back[52], S. Baker[57], V. Balagura[9,b], W. Baldini[18,44], A. Baranov[39], R.J. Barlow[58], G.C. Barrand[9], S. Barsuk[9], W. Barter[57], M. Bartolini[21], F. Baryshnikov[73], V. Batozskaya[33], B. Batsukh[63], A. Battig[12], V. Battista[45], A. Bay[45], F. Bedeschi[26], I. Bediaga[1], A. Beiter[63], L.J. Bel[29], S. Belin[24], N. Beliy[4], V. Bellee[45], N. Belloli[22,i], K. Belous[41], I. Belyaev[36], G. Bencivenni[20], E. Ben-Haim[10], S. Benson[29], S. Beranek[11], A. Berezhnoy[37], R. Bernet[46], D. Berninghoff[14], E. Bertholet[10], A. Bertolin[25], C. Betancourt[46], F. Betti[17,e], M.O. Bettler[51], Ia. Bezshyiko[46], S. Bhasin[50], J. Bhom[31], M.S. Bieker[12], S. Bifani[49], P. Billoir[10], A. Birnkraut[12], A. Bizzeti[19,u], M. Bjørn[59], M.P. Blago[44], T. Blake[52], F. Blanc[45], S. Blusk[63], D. Bobulska[55], V. Bocci[28], O. Boente Garcia[43], T. Boettcher[60], A. Bondar[40,x], N. Bondar[35], S. Borghi[58,44], M. Borisyak[39], M. Borsato[14], M. Boubdir[11], T.J.V. Bowcock[56], C. Bozzi[18,44], S. Braun[14], M. Brodski[44], J. Brodzicka[31], A. Brossa Gonzalo[52], D. Brundu[24,44], E. Buchanan[50], A. Buonaura[46], C. Burr[58], A. Bursche[24], J. Butter[29], J. Buytaert[44], W. Byczynski[44], S. Cadeddu[24], H. Cai[67], R. Calabrese[18,g], S. Cali[18], R. Calladine[49], M. Calvi[22,i], M. Calvo Gomez[42,m], A. Camboni[42,m], P. Campana[20], D.H. Campora Perez[44], L. Capriotti[17,e], A. Carbone[17,e], G. Carboni[27], R. Cardinale[21], A. Cardini[24], P. Carniti[22,i], K. Carvalho Akiba[2], G. Casse[56], M. Cattaneo[44], G. Cavallero[21], R. Cenci[26,p], D. Chamont[9], M.G. Chapman[50], M. Charles[10,44], Ph. Charpentier[44], G. Chatzikonstantinidis[49], M. Chefdeville[6], V. Chekalina[39], C. Chen[3], S. Chen[24], S.-G. Chitic[44], V. Chobanova[43], M. Chrzaszcz[44], A. Chubykin[35], P. Ciambrone[20], X. Cid Vidal[43], G. Ciezarek[44], F. Cindolo[17], P.E.L. Clarke[54], M. Clemencic[44], H.V. Cliff[51], J. Closier[44], V. Coco[44], J.A.B. Coelho[9], J. Cogan[8], E. Cogneras[7], L. Cojocariu[34], P. Collins[44], T. Colombo[44], A. Comerma-Montells[14], A. Contu[24], G. Coombs[44], S. Coquereau[42], G. Corti[44], C.M. Costa Sobral[52], B. Couturier[44], G.A. Cowan[54], D.C. Craik[60], A. Crocombe[52], M. Cruz Torres[1], R. Currie[54], C.L. Da Silva[78], E. Dall'Occo[29], J. Dalseno[43,v], C. D'Ambrosio[44], A. Danilina[36], P. d'Argent[14], A. Davis[58], O. De Aguiar Francisco[44], K. De Bruyn[44], S. De Capua[58], M. De Cian[45], J.M. De Miranda[1], L. De Paula[2], M. De Serio[16,d], P. De Simone[20], J.A. de Vries[29], C.T. Dean[55], W. Dean[77], D. Decamp[6], L. Del Buono[10], B. Delaney[51], H.-P. Dembinski[13], M. Demmer[12], A. Dendek[32], D. Derkach[74], O. Deschamps[7], F. Desse[9], F. Dettori[24], B. Dey[68], A. Di Canto[44], P. Di Nezza[20], S. Didenko[73], H. Dijkstra[44], F. Dordei[24], M. Dorigo[26,y], A.C. dos Reis[1], A. Dosil Suárez[43], L. Douglas[55], A. Dovbnya[47], K. Dreimanis[56], L. Dufour[44], G. Dujany[10], P. Durante[44], J.M. Durham[78], D. Dutta[58], R. Dzhelyadin[41,†], M. Dziewiecki[14], A. Dziurda[31], A. Dzyuba[35], S. Easo[53], U. Egede[57], V. Egorychev[36], S. Eidelman[40,x], S. Eisenhardt[54], U. Eitschberger[12], R. Ekelhof[12], L. Eklund[55], S. Ely[63], A. Ene[34], S. Escher[11], S. Esen[29], T. Evans[61], A. Falabella[17], C. Färber[44], N. Farley[49], S. Farry[56], D. Fazzini[22,i], M. Féo[44], P. Fernandez Declara[44], A. Fernandez Prieto[43], F. Ferrari[17,e], L. Ferreira Lopes[45], F. Ferreira Rodrigues[2], S. Ferreres Sole[29], M. Ferro-Luzzi[44], S. Filippov[38], R.A. Fini[16], M. Fiorini[18,g], M. Firlej[32], C. Fitzpatrick[44], T. Fiutowski[32], F. Fleuret[9,b], M. Fontana[44], F. Fontanelli[21,h], R. Forty[44], V. Franco Lima[56], M. Frank[44], C. Frei[44], J. Fu[23,q], W. Funk[44], E. Gabriel[54], A. Gallas Torreira[43], D. Galli[17,e], S. Gallorini[25], S. Gambetta[54], Y. Gan[3], M. Gandelman[2], P. Gandini[23], Y. Gao[3], L.M. Garcia Martin[76], J. García Pardiñas[46], B. Garcia Plana[43], J. Garra Tico[51], L. Garrido[42], D. Gascon[42], C. Gaspar[44], G. Gazzoni[7], D. Gerick[14], E. Gersabeck[58], M. Gersabeck[58], T. Gershon[52], D. Gerstel[8], Ph. Ghez[6], V. Gibson[51],

JHEP10(2019)124

O.G. Girard[45], P. Gironella Gironell[42], L. Giubega[34], K. Gizdov[54], V.V. Gligorov[10], C. Göbel[65], D. Golubkov[36], A. Golutvin[57,73], A. Gomes[1,a], I.V. Gorelov[37], C. Gotti[22,i], E. Govorkova[29], J.P. Grabowski[14], R. Graciani Diaz[42], L.A. Granado Cardoso[44], E. Graugés[42], E. Graverini[46], G. Graziani[19], A. Grecu[34], R. Greim[29], P. Griffith[24], L. Grillo[58], L. Gruber[44], B.R. Gruberg Cazon[59], C. Gu[3], E. Gushchin[38], A. Guth[11], Yu. Guz[41,44], T. Gys[44], T. Hadavizadeh[59], C. Hadjivasiliou[7], G. Haefeli[45], C. Haen[44], S.C. Haines[51], B. Hamilton[62], Q. Han[68], X. Han[14], T.H. Hancock[59], S. Hansmann-Menzemer[14], N. Harnew[59], T. Harrison[56], C. Hasse[44], M. Hatch[44], J. He[4], M. Hecker[57], K. Heinicke[12], A. Heister[12], K. Hennessy[56], L. Henry[76], M. Heß[70], J. Heuel[11], A. Hicheur[64], R. Hidalgo Charman[58], D. Hill[59], M. Hilton[58], P.H. Hopchev[45], J. Hu[14], W. Hu[68], W. Huang[4], Z.C. Huard[61], W. Hulsbergen[29], T. Humair[57], M. Hushchyn[74], D. Hutchcroft[56], D. Hynds[29], P. Ibis[12], M. Idzik[32], P. Ilten[49], A. Inglessi[35], A. Inyakin[41], K. Ivshin[35], R. Jacobsson[44], S. Jakobsen[44], J. Jalocha[59], E. Jans[29], B.K. Jashal[76], A. Jawahery[62], F. Jiang[3], M. John[59], D. Johnson[44], C.R. Jones[51], C. Joram[44], B. Jost[44], N. Jurik[59], S. Kandybei[47], M. Karacson[44], J.M. Kariuki[50], S. Karodia[55], N. Kazeev[74], M. Kecke[14], F. Keizer[51], M. Kelsey[63], M. Kenzie[51], T. Ketel[30], B. Khanji[44], A. Kharisova[75], C. Khurewathanakul[45], K.E. Kim[63], T. Kirn[11], V.S. Kirsebom[45], S. Klaver[20], K. Klimaszewski[33], S. Koliiev[48], M. Kolpin[14], R. Kopecna[14], P. Koppenburg[29], I. Kostiuk[29,48], O. Kot[48], S. Kotriakhova[35], M. Kozeiha[7], L. Kravchuk[38], M. Kreps[52], F. Kress[57], S. Kretzschmar[11], P. Krokovny[40,x], W. Krupa[32], W. Krzemien[33], W. Kucewicz[31,l], M. Kucharczyk[31], V. Kudryavtsev[40,x], G.J. Kunde[78], A.K. Kuonen[45], T. Kvaratskheliya[36], D. Lacarrere[44], G. Lafferty[58], A. Lai[24], D. Lancierini[46], G. Lanfranchi[20], C. Langenbruch[11], T. Latham[52], C. Lazzeroni[49], R. Le Gac[8], R. Lefèvre[7], A. Leflat[37], F. Lemaitre[44], O. Leroy[8], T. Lesiak[31], B. Leverington[14], H. Li[66], P.-R. Li[4,ab], X. Li[78], Y. Li[5], Z. Li[63], X. Liang[63], T. Likhomanenko[72], R. Lindner[44], F. Lionetto[46], V. Lisovskyi[9], G. Liu[66], X. Liu[3], D. Loh[52], A. Loi[24], I. Longstaff[55], J.H. Lopes[2], G. Loustau[46], G.H. Lovell[51], D. Lucchesi[25,o], M. Lucio Martinez[43], Y. Luo[3], A. Lupato[25], E. Luppi[18,g], O. Lupton[52], A. Lusiani[26], X. Lyu[4], F. Machefert[9], F. Maciuc[34], V. Macko[45], P. Mackowiak[12], S. Maddrell-Mander[50], O. Maev[35,44], K. Maguire[58], D. Maisuzenko[35], M.W. Majewski[32], S. Malde[59], B. Malecki[44], A. Malinin[72], T. Maltsev[40,x], H. Malygina[14], G. Manca[24,f], G. Mancinelli[8], D. Marangotto[23,q], J. Maratas[7,w], J.F. Marchand[6], U. Marconi[17], C. Marin Benito[9], M. Marinangeli[45], P. Marino[45], J. Marks[14], P.J. Marshall[56], G. Martellotti[28], M. Martinelli[44,22], D. Martinez Santos[43], F. Martinez Vidal[76], A. Massafferri[1], M. Materok[11], R. Matev[44], A. Mathad[46], Z. Mathe[44], V. Matiunin[36], C. Matteuzzi[22], K.R. Mattioli[77], A. Mauri[46], E. Maurice[9,b], B. Maurin[45], M. McCann[57,44], A. McNab[58], R. McNulty[15], J.V. Mead[56], B. Meadows[61], C. Meaux[8], N. Meinert[70], D. Melnychuk[33], M. Merk[29], A. Merli[23,q], E. Michielin[25], D.A. Milanes[69], E. Millard[52], M.-N. Minard[6], L. Minzoni[18,g], D.S. Mitzel[14], A. Mödden[12], A. Mogini[10], R.D. Moise[57], T. Mombächer[12], I.A. Monroy[69], S. Monteil[7], M. Morandin[25], G. Morello[20], M.J. Morello[26,t], J. Moron[32], A.B. Morris[8], R. Mountain[63], F. Muheim[54], M. Mukherjee[68], M. Mulder[29], D. Müller[44], J. Müller[12], K. Müller[46], V. Müller[12], C.H. Murphy[59], D. Murray[58], P. Naik[50], T. Nakada[45], R. Nandakumar[53], A. Nandi[59], T. Nanut[45], I. Nasteva[2], M. Needham[54], N. Neri[23,q], S. Neubert[14], N. Neufeld[44], R. Newcombe[57], T.D. Nguyen[45], C. Nguyen-Mau[45,n], S. Nieswand[11], R. Niet[12], N. Nikitin[37], N.S. Nolte[44], A. Oblakowska-Mucha[32], V. Obraztsov[41], S. Ogilvy[55], D.P. O'Hanlon[17], R. Oldeman[24,f], C.J.G. Onderwater[71], J.D. Osborn[77], A. Ossowska[31], J.M. Otalora Goicochea[2], T. Ovsiannikova[36], P. Owen[46], A. Oyanguren[76], P.R. Pais[45], T. Pajero[26,t], A. Palano[16], M. Palutan[20], G. Panshin[75], A. Papanestis[53], M. Pappagallo[54], L.L. Pappalardo[18,g], W. Parker[62], C. Parkes[58,44], G. Passaleva[19,44], A. Pastore[16], M. Patel[57], C. Patrignani[17,e], A. Pearce[44], A. Pellegrino[29], G. Penso[28], M. Pepe Altarelli[44], S. Perazzini[17], D. Pereima[36], P. Perret[7], L. Pescatore[45], K. Petridis[50], A. Petrolini[21,h], A. Petrov[72],

JHEP10(2019)124

S. Petrucci[54], M. Petruzzo[23,q], B. Pietrzyk[6], G. Pietrzyk[45], M. Pikies[31], M. Pili[59], D. Pinci[28], J. Pinzino[44], F. Pisani[44], A. Piucci[14], V. Placinta[34], S. Playfer[54], J. Plews[49], M. Plo Casasus[43], F. Polci[10], M. Poli Lener[20], M. Poliakova[63], A. Poluektov[8], N. Polukhina[73,c], I. Polyakov[63], E. Polycarpo[2], G.J. Pomery[50], S. Ponce[44], A. Popov[41], D. Popov[49,13], S. Poslavskii[41], E. Price[50], C. Prouve[43], V. Pugatch[48], A. Puig Navarro[46], H. Pullen[59], G. Punzi[26,p], W. Qian[4], J. Qin[4], R. Quagliani[10], B. Quintana[7], N.V. Raab[15], B. Rachwal[32], J.H. Rademacker[50], M. Rama[26], M. Ramos Pernas[43], M.S. Rangel[2], F. Ratnikov[39,74], G. Raven[30], M. Ravonel Salzgeber[44], M. Reboud[6], F. Redi[45], S. Reichert[12], F. Reiss[10], C. Remon Alepuz[76], Z. Ren[3], V. Renaudin[59], S. Ricciardi[53], S. Richards[50], K. Rinnert[56], P. Robbe[9], A. Robert[10], A.B. Rodrigues[45], E. Rodrigues[61], J.A. Rodriguez Lopez[69], M. Roehrken[44], S. Roiser[44], A. Rollings[59], V. Romanovskiy[41], A. Romero Vidal[43], J.D. Roth[77], M. Rotondo[20], M.S. Rudolph[63], T. Ruf[44], J. Ruiz Vidal[76], J.J. Saborido Silva[43], N. Sagidova[35], B. Saitta[24,f], V. Salustino Guimaraes[65], C. Sanchez Gras[29], C. Sanchez Mayordomo[76], B. Sanmartin Sedes[43], R. Santacesaria[28], C. Santamarina Rios[43], M. Santimaria[20,44], E. Santovetti[27,j], G. Sarpis[58], A. Sarti[20,k], C. Satriano[28,s], A. Satta[27], M. Saur[4], D. Savrina[36,37], S. Schael[11], M. Schellenberg[12], M. Schiller[55], H. Schindler[44], M. Schmelling[13], T. Schmelzer[12], B. Schmidt[44], O. Schneider[45], A. Schopper[44], H.F. Schreiner[61], M. Schubiger[45], S. Schulte[45], M.H. Schune[9], R. Schwemmer[44], B. Sciascia[20], A. Sciubba[28,k], A. Semennikov[36], E.S. Sepulveda[10], A. Sergi[49,44], N. Serra[46], J. Serrano[8], L. Sestini[25], A. Seuthe[12], P. Seyfert[44], M. Shapkin[41], T. Shears[56], L. Shekhtman[40,x], V. Shevchenko[72], E. Shmanin[73], B.G. Siddi[18], R. Silva Coutinho[46], L. Silva de Oliveira[2], G. Simi[25,o], S. Simone[16,d], I. Skiba[18], N. Skidmore[14], T. Skwarnicki[63], M.W. Slater[49], J.G. Smeaton[51], E. Smith[11], I.T. Smith[54], M. Smith[57], M. Soares[17], l. Soares Lavra[1], M.D. Sokoloff[61], F.J.P. Soler[55], B. Souza De Paula[2], B. Spaan[12], E. Spadaro Norella[23,q], P. Spradlin[55], F. Stagni[44], M. Stahl[14], S. Stahl[44], P. Stefko[45], S. Stefkova[57], O. Steinkamp[46], S. Stemmle[14], O. Stenyakin[41], M. Stepanova[35], H. Stevens[12], A. Stocchi[9], S. Stone[63], S. Stracka[26], M.E. Stramaglia[45], M. Straticiuc[34], U. Straumann[46], S. Strokov[75], J. Sun[3], L. Sun[67], Y. Sun[62], K. Swientek[32], A. Szabelski[33], T. Szumlak[32], M. Szymanski[4], Z. Tang[3], T. Tekampe[12], G. Tellarini[18], F. Teubert[44], E. Thomas[44], M.J. Tilley[57], V. Tisserand[7], S. T'Jampens[6], M. Tobin[5], S. Tolk[44], L. Tomassetti[18,g], D. Tonelli[26], D.Y. Tou[10], R. Tourinho Jadallah Aoude[1], E. Tournefier[6], M. Traill[55], M.T. Tran[45], A. Trisovic[51], A. Tsaregorodtsev[8], G. Tuci[26,44,p], A. Tully[51], N. Tuning[29], A. Ukleja[33], A. Usachov[9], A. Ustyuzhanin[39,74], U. Uwer[14], A. Vagner[75], V. Vagnoni[17], A. Valassi[44], S. Valat[44], G. Valenti[17], M. van Beuzekom[29], H. Van Hecke[78], E. van Herwijnen[44], C.B. Van Hulse[15], J. van Tilburg[29], M. van Veghel[29], R. Vazquez Gomez[44], P. Vazquez Regueiro[43], C. Vázquez Sierra[29], S. Vecchi[18], J.J. Velthuis[50], M. Veltri[19,r], A. Venkateswaran[63], M. Vernet[7], M. Veronesi[29], M. Vesterinen[52], J.V. Viana Barbosa[44], D. Vieira[4], M. Vieites Diaz[43], H. Viemann[70], X. Vilasis-Cardona[42,m], A. Vitkovskiy[29], M. Vitti[51], V. Volkov[37], A. Vollhardt[46], D. Vom Bruch[10], B. Voneki[44], A. Vorobyev[35], V. Vorobyev[40,x], N. Voropaev[35], R. Waldi[70], J. Walsh[26], J. Wang[5], M. Wang[3], Y. Wang[68], Z. Wang[46], D.R. Ward[51], H.M. Wark[56], N.K. Watson[49], D. Websdale[57], A. Weiden[46], C. Weisser[60], M. Whitehead[11], G. Wilkinson[59], M. Wilkinson[63], I. Williams[51], M. Williams[60], M.R.J. Williams[58], T. Williams[49], F.F. Wilson[53], M. Winn[9], W. Wislicki[33], M. Witek[31], G. Wormser[9], S.A. Wotton[51], K. Wyllie[44], D. Xiao[68], Y. Xie[68], H. Xing[66], A. Xu[3], M. Xu[68], Q. Xu[4], Z. Xu[6], Z. Xu[3], Z. Yang[3], Z. Yang[62], Y. Yao[63], L.E. Yeomans[56], H. Yin[68], J. Yu[68,aa], X. Yuan[63], O. Yushchenko[41], K.A. Zarebski[49], M. Zavertyaev[13,c], M. Zeng[3], D. Zhang[68], L. Zhang[3], W.C. Zhang[3,z], Y. Zhang[44], A. Zhelezov[14], Y. Zheng[4], X. Zhu[3], V. Zhukov[11,37], J.B. Zonneveld[54], S. Zucchelli[17,e]

[1] *Centro Brasileiro de Pesquisas Físicas (CBPF), Rio de Janeiro, Brazil*

[2] *Universidade Federal do Rio de Janeiro (UFRJ), Rio de Janeiro, Brazil*

JHEP10(2019)124

[3] Center for High Energy Physics, Tsinghua University, Beijing, China
[4] University of Chinese Academy of Sciences, Beijing, China
[5] Institute Of High Energy Physics (ihep), Beijing, China
[6] Univ. Grenoble Alpes, Univ. Savoie Mont Blanc, CNRS, IN2P3-LAPP, Annecy, France
[7] Université Clermont Auvergne, CNRS/IN2P3, LPC, Clermont-Ferrand, France
[8] Aix Marseille Univ, CNRS/IN2P3, CPPM, Marseille, France
[9] LAL, Univ. Paris-Sud, CNRS/IN2P3, Université Paris-Saclay, Orsay, France
[10] LPNHE, Sorbonne Université, Paris Diderot Sorbonne Paris Cité, CNRS/IN2P3, Paris, France
[11] I. Physikalisches Institut, RWTH Aachen University, Aachen, Germany
[12] Fakultät Physik, Technische Universität Dortmund, Dortmund, Germany
[13] Max-Planck-Institut für Kernphysik (MPIK), Heidelberg, Germany
[14] Physikalisches Institut, Ruprecht-Karls-Universität Heidelberg, Heidelberg, Germany
[15] School of Physics, University College Dublin, Dublin, Ireland
[16] INFN Sezione di Bari, Bari, Italy
[17] INFN Sezione di Bologna, Bologna, Italy
[18] INFN Sezione di Ferrara, Ferrara, Italy
[19] INFN Sezione di Firenze, Firenze, Italy
[20] INFN Laboratori Nazionali di Frascati, Frascati, Italy
[21] INFN Sezione di Genova, Genova, Italy
[22] INFN Sezione di Milano-Bicocca, Milano, Italy
[23] INFN Sezione di Milano, Milano, Italy
[24] INFN Sezione di Cagliari, Monserrato, Italy
[25] INFN Sezione di Padova, Padova, Italy
[26] INFN Sezione di Pisa, Pisa, Italy
[27] INFN Sezione di Roma Tor Vergata, Roma, Italy
[28] INFN Sezione di Roma La Sapienza, Roma, Italy
[29] Nikhef National Institute for Subatomic Physics, Amsterdam, Netherlands
[30] Nikhef National Institute for Subatomic Physics and VU University Amsterdam, Amsterdam, Netherlands
[31] Henryk Niewodniczanski Institute of Nuclear Physics Polish Academy of Sciences, Kraków, Poland
[32] AGH — University of Science and Technology, Faculty of Physics and Applied Computer Science, Kraków, Poland
[33] National Center for Nuclear Research (NCBJ), Warsaw, Poland
[34] Horia Hulubei National Institute of Physics and Nuclear Engineering, Bucharest-Magurele, Romania
[35] Petersburg Nuclear Physics Institute (PNPI), Gatchina, Russia
[36] Institute of Theoretical and Experimental Physics (ITEP), Moscow, Russia
[37] Institute of Nuclear Physics, Moscow State University (SINP MSU), Moscow, Russia
[38] Institute for Nuclear Research of the Russian Academy of Sciences (INR RAS), Moscow, Russia
[39] Yandex School of Data Analysis, Moscow, Russia
[40] Budker Institute of Nuclear Physics (SB RAS), Novosibirsk, Russia
[41] Institute for High Energy Physics (IHEP), Protvino, Russia
[42] ICCUB, Universitat de Barcelona, Barcelona, Spain
[43] Instituto Galego de Física de Altas Enerxías (IGFAE), Universidade de Santiago de Compostela, Santiago de Compostela, Spain
[44] European Organization for Nuclear Research (CERN), Geneva, Switzerland
[45] Institute of Physics, Ecole Polytechnique Fédérale de Lausanne (EPFL), Lausanne, Switzerland
[46] Physik-Institut, Universität Zürich, Zürich, Switzerland
[47] NSC Kharkiv Institute of Physics and Technology (NSC KIPT), Kharkiv, Ukraine
[48] Institute for Nuclear Research of the National Academy of Sciences (KINR), Kyiv, Ukraine
[49] University of Birmingham, Birmingham, United Kingdom
[50] H.H. Wills Physics Laboratory, University of Bristol, Bristol, United Kingdom

JHEP10(2019)124

[51] Cavendish Laboratory, University of Cambridge, Cambridge, United Kingdom
[52] Department of Physics, University of Warwick, Coventry, United Kingdom
[53] STFC Rutherford Appleton Laboratory, Didcot, United Kingdom
[54] School of Physics and Astronomy, University of Edinburgh, Edinburgh, United Kingdom
[55] School of Physics and Astronomy, University of Glasgow, Glasgow, United Kingdom
[56] Oliver Lodge Laboratory, University of Liverpool, Liverpool, United Kingdom
[57] Imperial College London, London, United Kingdom
[58] School of Physics and Astronomy, University of Manchester, Manchester, United Kingdom
[59] Department of Physics, University of Oxford, Oxford, United Kingdom
[60] Massachusetts Institute of Technology, Cambridge, MA, United States
[61] University of Cincinnati, Cincinnati, OH, United States
[62] University of Maryland, College Park, MD, United States
[63] Syracuse University, Syracuse, NY, United States
[64] Laboratory of Mathematical and Subatomic Physics, Constantine, Algeria, associated to [2]
[65] Pontifícia Universidade Católica do Rio de Janeiro (PUC-Rio), Rio de Janeiro, Brazil, associated to [2]
[66] South China Normal University, Guangzhou, China, associated to [3]
[67] School of Physics and Technology, Wuhan University, Wuhan, China, associated to [3]
[68] Institute of Particle Physics, Central China Normal University, Wuhan, Hubei, China, associated to [3]
[69] Departamento de Fisica, Universidad Nacional de Colombia, Bogota, Colombia, associated to [10]
[70] Institut für Physik, Universität Rostock, Rostock, Germany, associated to [14]
[71] Van Swinderen Institute, University of Groningen, Groningen, Netherlands, associated to [29]
[72] National Research Centre Kurchatov Institute, Moscow, Russia, associated to [36]
[73] National University of Science and Technology "MISIS", Moscow, Russia, associated to [36]
[74] National Research University Higher School of Economics, Moscow, Russia, associated to [39]
[75] National Research Tomsk Polytechnic University, Tomsk, Russia, associated to [36]
[76] Instituto de Fisica Corpuscular, Centro Mixto Universidad de Valencia — CSIC, Valencia, Spain, associated to [42]
[77] University of Michigan, Ann Arbor, United States, associated to [63]
[78] Los Alamos National Laboratory (LANL), Los Alamos, United States, associated to [63]

[a] Universidade Federal do Triângulo Mineiro (UFTM), Uberaba-MG, Brazil
[b] Laboratoire Leprince-Ringuet, Palaiseau, France
[c] P.N. Lebedev Physical Institute, Russian Academy of Science (LPI RAS), Moscow, Russia
[d] Università di Bari, Bari, Italy
[e] Università di Bologna, Bologna, Italy
[f] Università di Cagliari, Cagliari, Italy
[g] Università di Ferrara, Ferrara, Italy
[h] Università di Genova, Genova, Italy
[i] Università di Milano Bicocca, Milano, Italy
[j] Università di Roma Tor Vergata, Roma, Italy
[k] Università di Roma La Sapienza, Roma, Italy
[l] AGH — University of Science and Technology, Faculty of Computer Science, Electronics and Telecommunications, Kraków, Poland
[m] LIFAELS, La Salle, Universitat Ramon Llull, Barcelona, Spain
[n] Hanoi University of Science, Hanoi, Vietnam
[o] Università di Padova, Padova, Italy
[p] Università di Pisa, Pisa, Italy
[q] Università degli Studi di Milano, Milano, Italy
[r] Università di Urbino, Urbino, Italy
[s] Università della Basilicata, Potenza, Italy

JHEP10(2019)124

[t] *Scuola Normale Superiore, Pisa, Italy*
[u] *Università di Modena e Reggio Emilia, Modena, Italy*
[v] *H.H. Wills Physics Laboratory, University of Bristol, Bristol, United Kingdom*
[w] *MSU — Iligan Institute of Technology (MSU-IIT), Iligan, Philippines*
[x] *Novosibirsk State University, Novosibirsk, Russia*
[y] *Sezione INFN di Trieste, Trieste, Italy*
[z] *School of Physics and Information Technology, Shaanxi Normal University (SNNU), Xi'an, China*
[aa] *Physics and Micro Electronic College, Hunan University, Changsha City, China*
[ab] *Lanzhou University, Lanzhou, China*

[†] *Deceased*

JHEP10(2019)124